

1 **Identification of small molecular chaperones binding P23H mutant opsin through an *in silico***
2 **structure-based approach**

3
4 Francesca Picarazzi,¹ Marika Zuanon,² Gaia Pasqualetto,³ Silvia Cammarone,⁴ Isabella Romeo,⁴
5 Mark T. Young,² Andrea Brancale,^{3,5} Marcella Bassetto,⁶ Mattia Mori^{1*}

6
7 ¹ Department of Biotechnology, Chemistry and Pharmacy, University of Siena, Via Aldo Moro 2,
8 53100 Siena, Italy.

9 ² School of Biosciences, Cardiff University, Cardiff CF10 3AX, UK

10 ³ School of Pharmacy and Pharmaceutical Sciences, Cardiff University, Cardiff CF10 3NB, UK

11 ⁴ Dipartimento di Chimica e Tecnologie del Farmaco, Facoltà di Farmacia e Medicina, "Sapienza"
12 Università di Roma, P. le Aldo Moro 5, 00185 Roma, Italy.

13 ⁵ Vysoká Škola Chemiko-Technologická v Praze, Prague, Czech Republic

14 ⁶ Department of Chemistry, Faculty of Science and Engineering, Swansea University, Swansea SA2
15 8PP, UK

16
17
18
19 **Corresponding author:**

20 Prof. Mattia Mori, Department of Biotechnology, Chemistry and Pharmacy, University of Siena,
21 Via Aldo Moro 2, 53100 Siena, Italy. Phone: +39 0577232360. E-mail address:
22 mattia.mori@unisi.it

23 **Abstract**

24 The N-terminal P23H opsin mutation accounts for most of *retinitis pigmentosa* (RP) cases. P23H
25 functions and folding can be rescued by small chaperone ligands, which contributes to validate
26 mutant opsin as a suitable target for pharmacological treatment of RP. However, the lack of
27 structural details on P23H mutant opsin strongly impairs drug design, and new chemotypes of
28 effective chaperones of P23H opsin are in high demand.

29 Here, a computational-boosted workflow combining homology modeling with molecular dynamics
30 (MD) simulations and virtual screening was used to select putative P23H opsin chaperones among
31 different libraries through a structure-based approach. *In vitro* studies corroborated the reliability of
32 the structural model generated in this work, and identified a number of novel chemotypes of safe
33 and effective chaperones able to promote P23H opsin trafficking to the outer cell membrane.

34

35

36

37

38

39

40

41

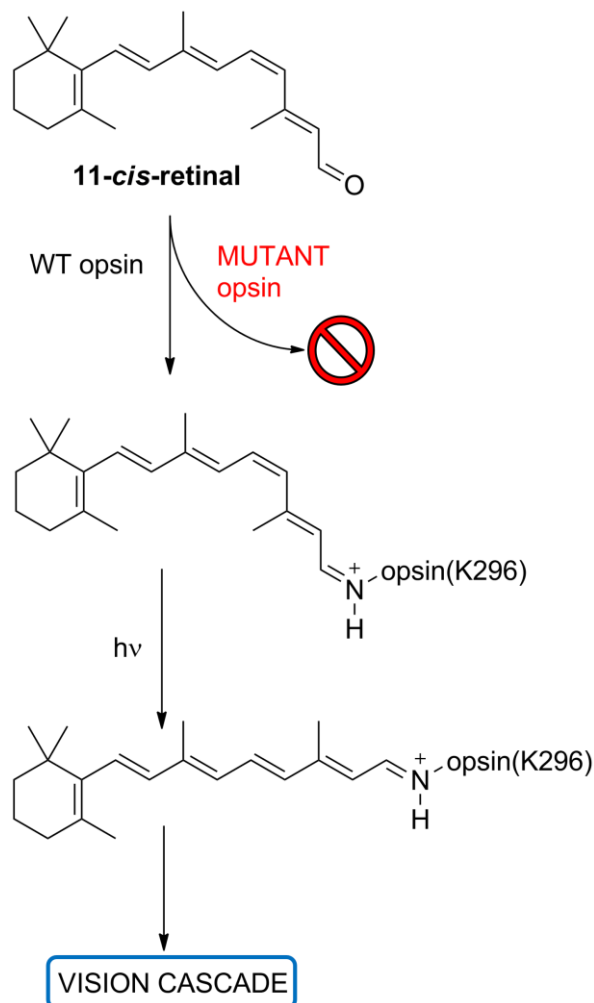
42

43

44

45 **Introduction**

46 Rhodopsin is a G protein-coupled receptor (GPCR) membrane protein that is activated by light of
47 different wavelengths in organisms ranging from single-cell eubacteria and archaea to humans. In
48 vertebrates, rhodopsin is responsible for vision, a process triggered by light-induced
49 photoisomerization of the retinal chromophore from its 11-*cis* to the all-*trans* form (Figure 1).
50 When bound to opsin forming rhodopsin, the retinal cofactor is covalently linked to the side chain
51 of K296 through a protonated Schiff base. Retinal photoisomerization induces a number of
52 conformational modifications to rhodopsin that finally activate the vision transduction cascade
53 (Figure 1).¹⁻³ Proper folding and localization of rhodopsin in the outer segment (OS) of
54 photoreceptor cells is essential to vision. In this context, opsin mutations are among the most
55 common cause of inherited ocular diseases, including *retinitis pigmentosa* (RP).⁴⁻⁶

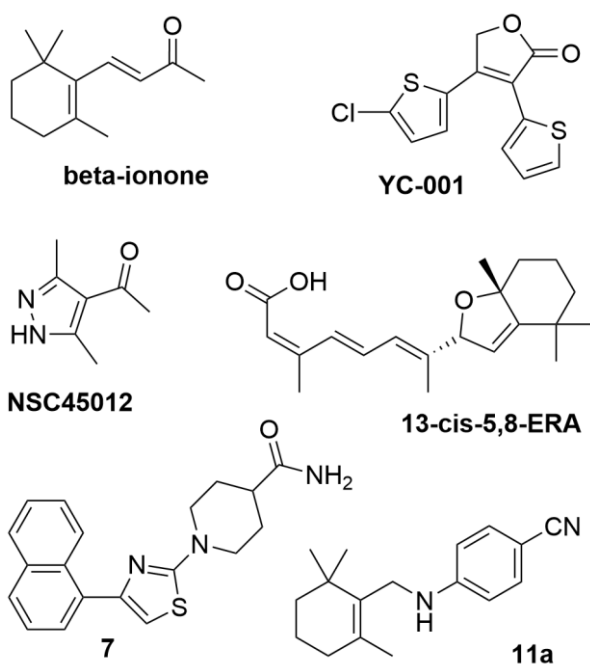


57 **Figure 1.** Chemical structure of the visual pigment chromophore 11-*cis*-retinal and its
58 photoisomerization to the all-*trans* form when bound to K296 of opsin.

59 The P23H mutation in the N-terminal tail of opsin causes structural destabilization and impairs the
60 correct protein folding and binding to the natural chromophore 11-*cis*-retinal, accounting for most
61 of RP cases with prevalence in North America (~10% of RP cases).⁷⁻¹⁰ In addition, incorrect
62 protein folding can also be caused by low cellular levels of 11-*cis*-retinal, which in these conditions
63 is unable to satisfactorily function as a molecular chaperone for opsin. Several lines of evidence
64 show that misfolded opsin is poorly translocated to the OS and accumulates in the endoplasmic
65 reticulum (ER) where it causes aggregation and cellular degradation.¹¹⁻¹³ Although the precise
66 mechanisms leading to photoreceptor degradation and disease development are not yet elucidated,
67 recent *in vitro* studies showed that the correct folding and trafficking of P23H mutant opsin can be
68 partially rescued by small chaperone ligands, i.e., small molecules able to bind misfolded P23H
69 opsin and restore the native conformational state of wild-type (WT) rhodopsin as well as to promote
70 the correct receptor localization in the OS.^{14, 15} Encouraged by the beneficial effects of 11-*cis*-retinal
71 administration in an early clinical trial,¹⁶ a number of retinal analogues have been developed.¹⁷⁻²⁰
72 However, these molecules bear major limitations associated to the photoinduced isomerization that
73 can occur also during the protein synthesis in the ER, leading to protein instability.²¹ While binding
74 and opsin chaperone properties of the retinal derivative beta-ionone (Figure 2) have long been
75 known,^{22, 23} non-retinoid chaperones are highly needed as they are expected to overcome the
76 limitations of retinoids, and to be more suitable candidates for drug development. Nevertheless, the
77 lack of high-resolution structural details on opsin mutants strongly hampers the rational design of
78 effective chaperones.²⁴ At present, very few non-retinoid chaperones of P23H opsin have been
79 disclosed, most still at a development stage that is far from translational or clinical applications.
80 One of the most widely used small molecule chaperones of P23H opsin is the non-retinoid
81 compound named **YC-001** (Figure 2), a 2,5-dihydrofuran-2-one derivative discovered by a cell-

82 based high-throughput screen, which proved able to bind non-covalently to P23H opsin and rescue
83 its trafficking to the membrane with *in vivo* efficacy.^{21, 25}

84 Computational tools proved highly effective in the discovery of novel small molecular chaperones
85 of mutant opsin. **NSC45012** [1-(3,5-dimethyl-1H-pyrazol-4-yl)ethanone] (Figure 2) is a weak
86 inhibitor of opsin regeneration providing 40% rescue of the mutant opsin, which has been
87 discovered through the docking-based virtual screening of a drug-like library of around 24,000
88 small molecules.²⁶ Moreover, the reversible orthosteric inhibitor of retinal binding **13-cis-5,8-ERA**
89 (Figure 2) has been discovered by virtually screening a library of more than 300,000 anionic
90 compounds followed by *in vitro* validation.²⁰ Recently, part of our group has carried out structure-
91 and ligand-based computational studies that have led to the identification of structural and
92 pharmacophoric features that are relevant for a molecule to stabilize the 9-*cis*- or the 11-*cis*-
93 retinal/opsin complex as well as to chaperone mutant opsin to be further developed as therapeutics
94 for RP (i.e., compounds **7** and **11a**, Figure 2).^{27, 28}



96

97 **Figure 2.** Chemical structure of reference chaperones of mutant opsin.

99 Here, boosted by our interest in the development of effective P23H opsin chaperones, and taking
100 advantage of computer-aided molecular simulations, we overcame the gap of reliable structural
101 information on the P23H opsin mutant to allow structure-guided drug design approaches.
102 Specifically, the structure of P23H mutant in complex with 11-*cis*-retinal was generated by
103 homology modeling while its conformational behavior was studied throughout molecular dynamics
104 (MD) simulations. Then, a representative MD frame extracted by cluster analysis was used as a
105 rigid receptor in a structure-based virtual screening to identify new small molecules that could bind
106 within the retinal binding site of P23H mutant opsin. To explore a wider portion of the chemical
107 space including commercial and natural compounds, and approved drugs, different libraries were
108 screened *in silico*. Cytotoxicity and the ability of virtual hits to promote mutant opsin relocalization
109 were investigated *in vitro*, corroborating computational predictions.

110

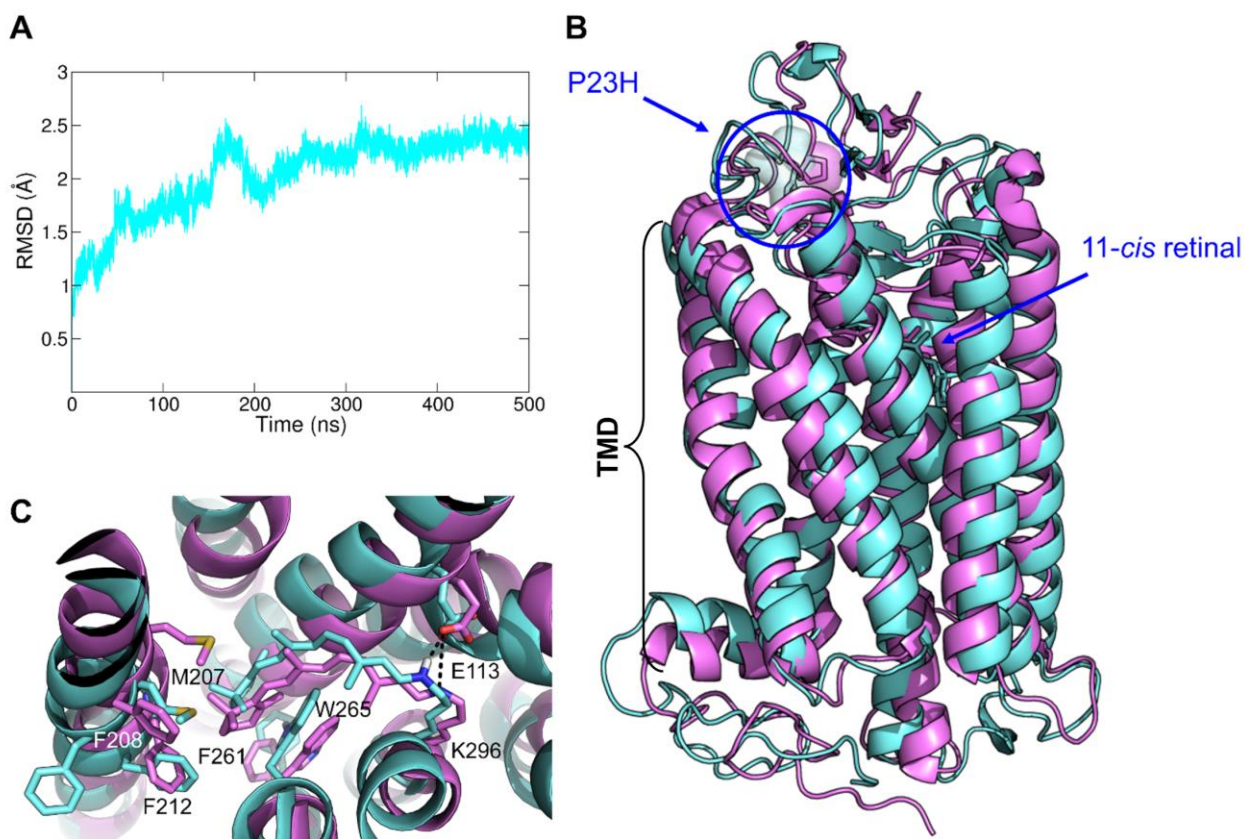
111 **Results and discussion**

112 **Homology modeling of P23H mutant rhodopsin receptor**

113 The full-length 3D structure of the P23H rhodopsin mutant was generated by homology modeling.
114 The high-resolution crystallographic structure of the bovine full-length rhodopsin (Protein Data
115 Bank²⁹ accession code PDB-ID: 1U19³⁰) was selected as a template. Analysis of the all-atom root
116 mean square deviation (RMSD) of the P23H mutant rhodopsin homology model along MD
117 trajectory confirmed that the protein conformation is stable during the last 200 ns (Figure 3A),
118 which suggests that the system achieved geometric convergence in MD simulations. Cluster
119 analysis of MD trajectories was then used to identify the centroid frame of the most populated
120 cluster, being represented by 86% of MD frames, which was used for analysis purposes. For the
121 sake of clarity, MD frames were grouped by a hierarchical agglomerative algorithm using distance
122 between frames calculated via best-fit coordinate RMSD as the distance metric; the representative

123 frame described herein corresponds to the centroid of the most populated cluster, i.e., the frame
124 having the lowest RMSD to every other frame in the cluster. Although the P23H mutation is
125 relatively distant from the binding site of 11-*cis*-retinal (approximately 16 Å) (Figure 3B), by
126 comparing the crystallographic structure of WT rhodopsin used as structural template with the
127 representative MD frame of the P23H rhodopsin extracted by cluster analysis, it is evident that the
128 P23H mutation affects mainly the structure of the transmembrane domain (TMD), whereas the
129 conformation of the 11-*cis*-retinal binding site is only marginally affected (Figure 3C). The
130 representative MD frame of P23H rhodopsin was finally selected as a receptor for subsequent
131 structure-based simulations because it describes the mutant system of interest in physiological
132 conditions compared to X-ray structures of the WT form.

133



134

135 **Figure 3.** A) All-atom RMSD of the P23H mutant opsin in complex with 11-*cis*-retinal cofactor. B)
136 Structural superposition of crystallographic structures of WT rhodopsin (PDB-ID 1U19) (pink) and

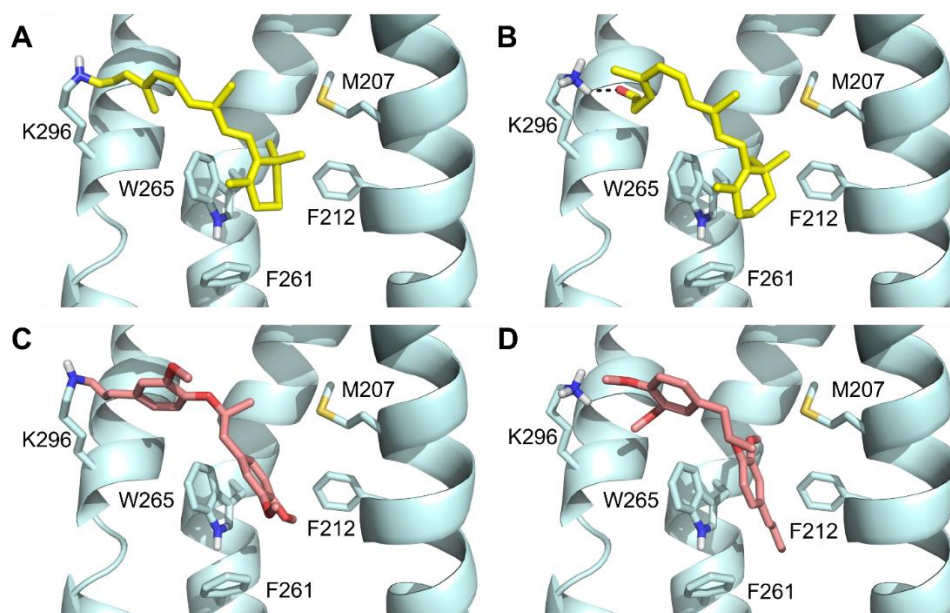
137 P23H mutant rhodopsin (cyan) depicted in front view, and C) close-up view of the 11-*cis*-retinal
138 binding site. Protein structures are aligned and showed in cartoon. The 11-*cis*-retinal chromophore
139 and the residues of interest are represented as sticks, while polar interactions are highlighted by
140 black dashed lines.

141

142 **Docking-based virtual screening**

143 Virtual screening was aimed at identifying small molecular chaperones that might potentially bind
144 the 11-*cis*-retinal site of the P23H mutant opsin. Specifically, these molecules should ideally
145 compete with the natural substrate, which is known to bind pathological opsin mutants with weak
146 affinity, and to restore opsin folding, functions and trafficking to the OS, as underlined by *in vitro*
147 studies.²⁰ Different libraries of compounds were selected for virtual screening, including: *i*) a high
148 diversity *in house* library of around 1,000 natural products, *ii*) the DrugBank database (around
149 2,509 approved drugs),³¹ and *iii*) the commercially available MolPort database (around 8 million
150 compounds).³² Natural products are a unique and privileged source of hit/lead compounds with a
151 wide chemical diversity as well as tools for understanding the chemical biology of protein targets.³³
152 ³⁴ In this context, natural products are largely used in virtual screening and drug design approaches
153 run by our research group, showing remarkable pharmacological activities mostly as antiviral or
154 anti-cancer drug candidates.³⁴⁻⁴⁰ The DrugBank database was selected with the purpose of
155 repositioning approved drugs, which is a widely used strategy that allows the therapeutic
156 exploitation of a drug for a therapeutic indication that is different from that of its approval.⁴¹⁻⁴³
157 Finally, the MolPort database is a rich source of commercially available diverse structures for
158 screening purposes. While screening libraries *i*) and *ii*) was achieved at a relatively low
159 computation cost, screening the MolPort database containing around 8 million compounds might
160 require much more time and resources to be completed. Given the presence of an aldehyde group in
161 the natural chromophore 11-*cis*-retinal, and to restrict the searchable chemical space, the MolPort

162 database was preliminarily filtered to identify compounds bearing up to three aldehyde groups,
163 leading to the generation of a sub-library containing 3,195 commercially available aldehydes.
164 All compounds (i.e., natural products, approved drugs, and aldehyde derivatives) were docked
165 within the 11-*cis*-retinal binding site of P23H opsin generated by MD simulations. The validity of
166 the docking/scoring function was preliminarily assessed by covalently and non-covalently re-
167 docking 11-*cis*-retinal in its binding site, which provided highly similar binding modes (Figure 4A
168 and 4B). In non-covalent docking, the oxygen atom from the aldehyde group is oriented towards
169 K296. In both docking settings, hydrophobic interactions of the ionone moiety with residues M207,
170 F212, F261, and W265 were preserved as in the crystallographic structure of WT rhodopsin.



171

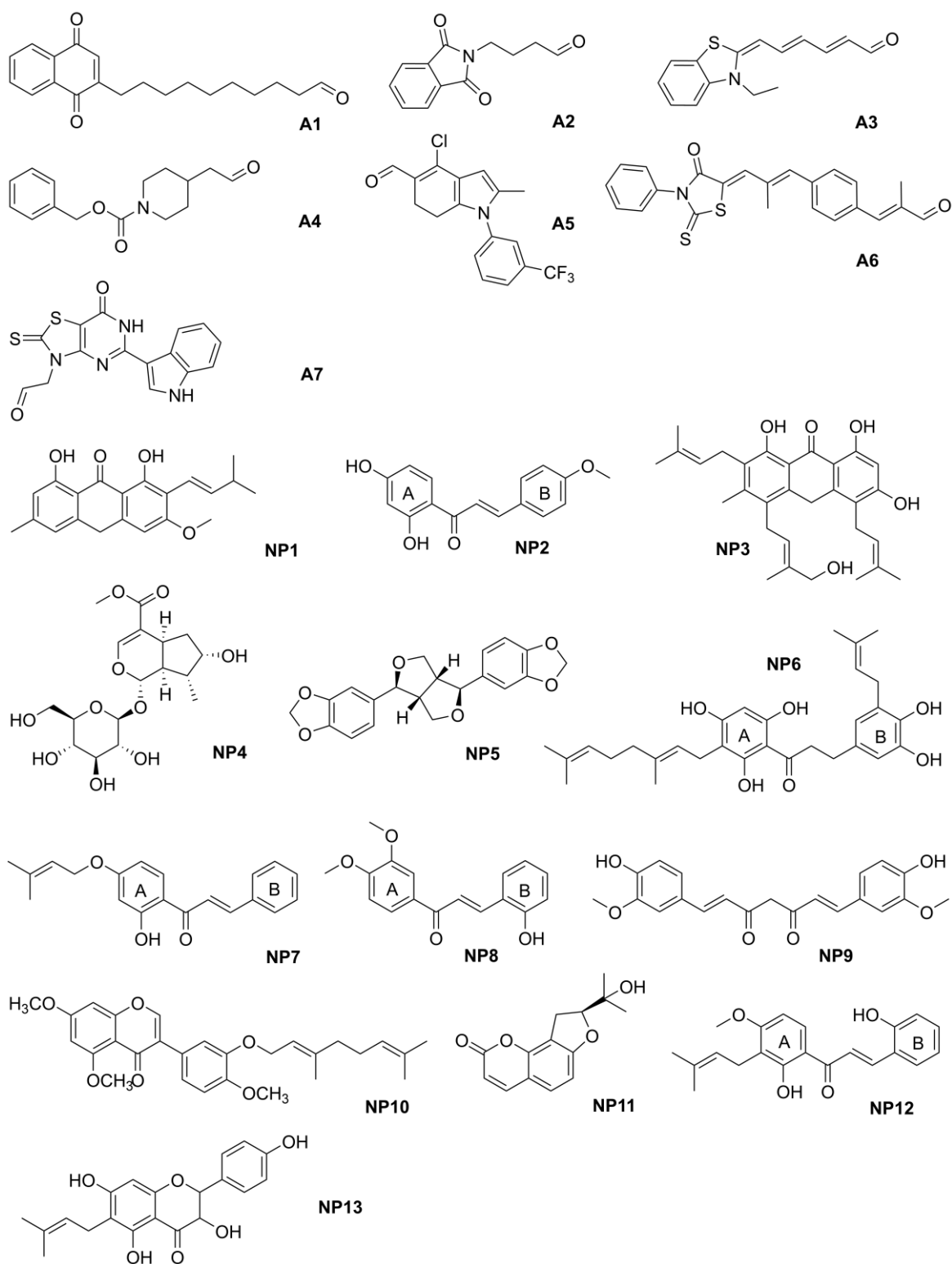
172 **Figure 4.** Predicted binding poses of 11-*cis*-retinal (yellow) and the MolPort 019-937-085
173 compound (pink) within the main chromophore binding site of the P23H opsin mutant, predicted by
174 covalent docking (A and C) and non-covalent docking (B and D). Polar interactions are highlighted
175 by black dashed lines. MolPort 019-937-085 was used as a negative control.

176

177 Docked molecules were sorted according to their scoring value, and the binding mode to P23H
178 opsin of the 100 top-ranked virtual hits from each library was visually inspected. In the case of

179 aldehydes, the covalent docking pose bound to K296 was compared with the non-covalent pose, this
180 latter mimicking the opsin/ligand recognition process within the retinal binding site. Similar to 11-
181 *cis*-retinal (Figure 4A), aldehydes sharing a comparable orientation and binding mode by covalent
182 and non-covalent docking were selected, while all others were discarded and not processed further
183 including *in vitro* tests. As an example of a discarded aldehyde, the compound characterized by
184 MolPort accession code 019-937-085 showed an opposite binding mode in covalent and non-
185 covalent docking (Figure 4C and 4D). Indeed, in covalent docking, the aldehyde group is bound to
186 K296 through a protonated Schiff base, with the dimethoxybenzene moiety oriented toward helices
187 6 and 5. In non-covalent docking, the aldehyde group points toward helices 5 and 6 (Figure 4C and
188 4D).

189 Finally, 7 aldehydes (**A1-A7**) and 13 natural products (**NP1-NP13**) were selected for experimental
190 validation (Figure 5). Unfortunately, no molecules from the DrugBank database exhibited an
191 interesting profile in binding to P23H opsin *in silico*, thus none of the approved drugs included in
192 this database was selected for further investigations.



193

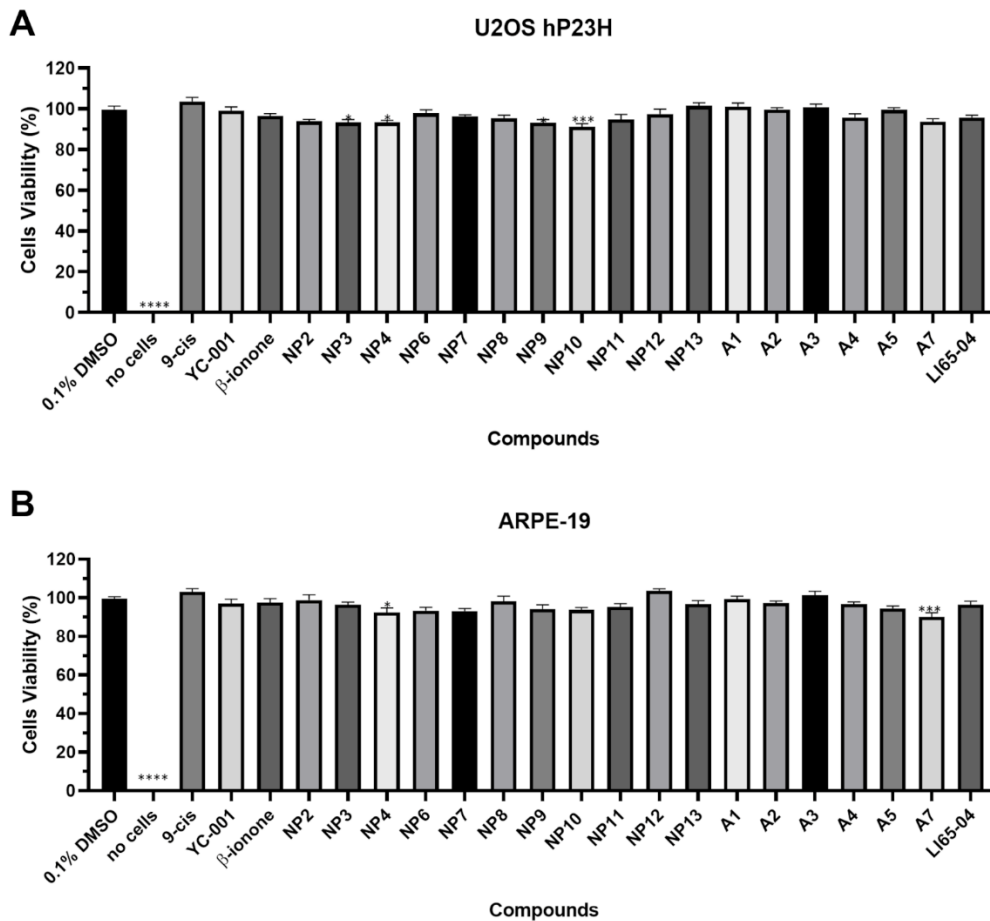
194 **Figure 5.** Chemical structure of putative small molecular chaperones binding the P23H mutant
 195 rhodopsin selected for *in vitro* evaluation. To facilitate further understanding of binding modes
 196 description, ring labels are added to chalcone derivatives.

197

198 **Cell viability assay**

199 The cytotoxicity of the screened compounds was tested in two different cell lines, U2OS and
200 ARPE-19. U2OS cell line transfected with human P23H his-tagged opsin is the cellular model used
201 in this study to determine compounds activity.^{27, 28} ARPE-19 cells are retinal pigmented epithelial
202 cells, that can be considered as a model to evaluate toxicity at the eye level.^{27, 28}

203 Most of the compounds appeared to be not toxic at 10 μ M, especially when tested on ARPE-19
204 cells. Only two compounds, **NP4** and **A7**, diminish cell viability by around 10%. **NP4** seems to be
205 cytotoxic by the same amount also on U2OS cells, along with **NP3**, **NP9** and **NP10** (Figure 6).
206 Overall, cell viability for both cell lines is not lower than 90% with any of the test compounds,
207 suggesting they are all suitable for activity evaluation in U2OS systems as potential therapeutics for
208 eye diseases.



209

210 **Figure 6.** Cytotoxicity evaluation of the screened compounds tested at 10 μ M on A) U2OS hP23H
 211 and B) ARPE-19 cells. Cell viability was determined as percentage calculated on the vehicle treated
 212 cells (0.1% DMSO). The bars represent the mean \pm SEM from three independent experimental
 213 repeats. Data were analysed using one-way ANOVA, Dunnett test, comparing the mean of each
 214 column bar with the vehicle, 0.1 % DMSO (**** $p < 0.0001$, *** $p < 0.001$, * $p < 0.03$). Wells
 215 containing diluted reagent with media, and without the presence of cells was considered as negative
 216 control.

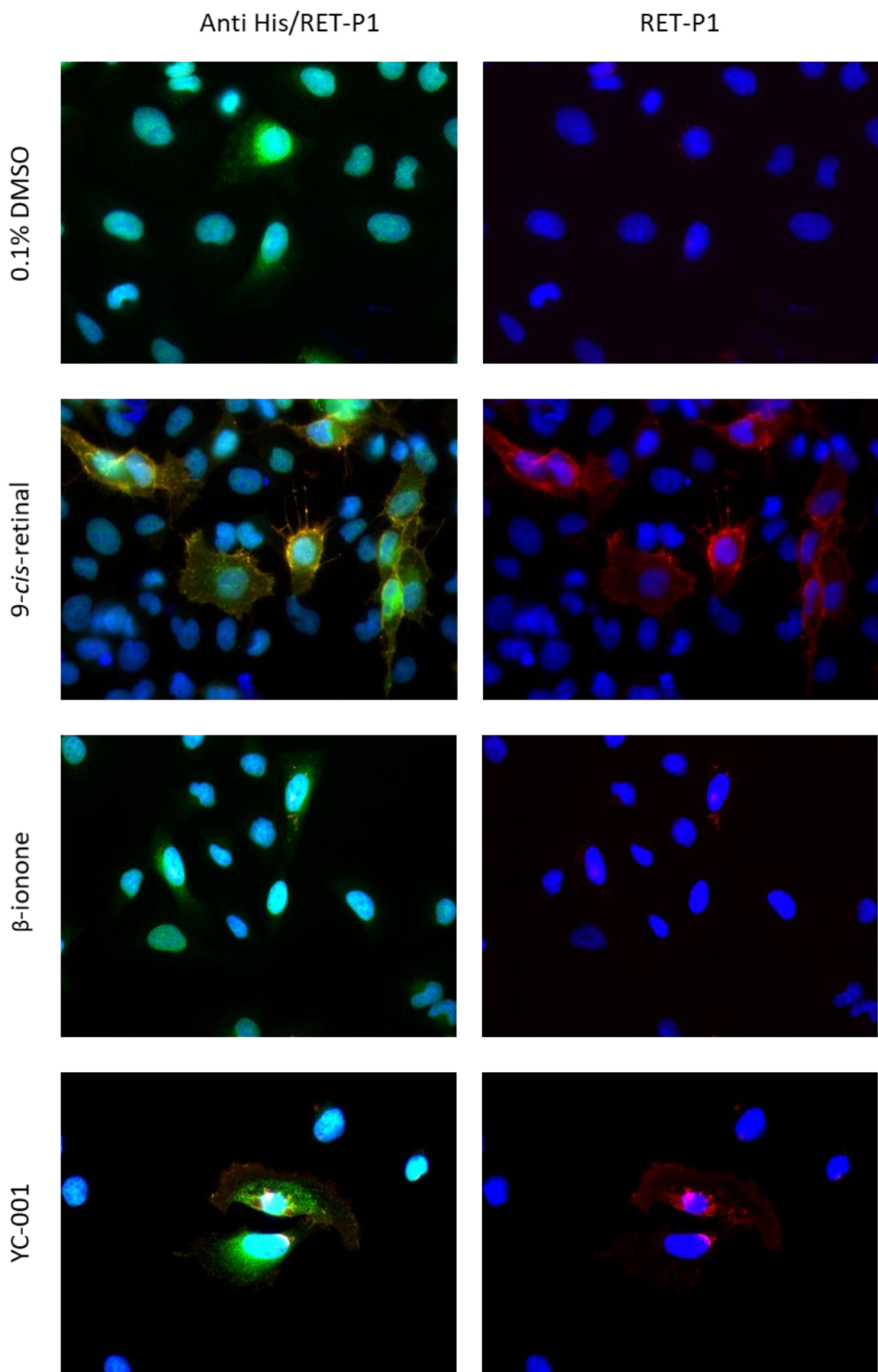
217

218 **Single cell fluorescent microscopy**

219 U2OS cells transfected with hP23H opsin (His-tag) were used to determine the ability of the
 220 compounds to promote opsin trafficking to the membrane.²⁸ The production of hP23H opsin is only
 221 induced in these U2OS cells when exposed to tetracycline. However, opsin bearing this mutation is

222 misfolded and accumulates in the cytoplasm if it is not bound to 9-*cis*-retinal forming isorhodopsin.
223 9-*cis*-Retinal is an analogue of endogenous 11-*cis*-retinal, which stabilizes opsin structure and
224 promotes its trafficking to the outer cell membrane (Figure 7).^{1, 44}

225 To evaluate opsin localization in U2OS cells, two antibodies were used. RET-P1 antibody, bound to
226 the secondary antibody AlexaFluor555 (red signal), binds opsin on its extracellular domain,
227 identifying this protein when localized at the membrane; instead, the His-tag antibody, bound to
228 AlexaFluor488 (green signal), recognizes the his-tag of the transfected opsin, detecting the total
229 opsin expressed by cells after tetracycline induction. In this way, an active compound would present
230 both the red and green signals, as 9-*cis*-retinal does, and an inactive one would present only the
231 green signal, related to total opsin, as the vehicle 0.1% DMSO does (Figure 7).



233

234 **Figure 7.** hP23H subcellular localization after U2OS treatment with the negative (0.1% DMSO)
235 and positive controls (*9-cis*-retinal, beta-ionone, and **YC-001**). *9-cis*-retinal was tested at 5 μ M (as
236 previously reported)²⁶, whereas beta-ionone, and **YC-001** at 10 μ M. Anti-His/RET-P1 refers to the
237 images merged from RET-P1 (red), and Anti-His tag (green) staining. Instead, RET-P1 refers to the
238 images obtained from the single RET-P1 staining. RET-P1 detects opsin protein expressed at the
239 membrane, binding its extracellular epitope, while Anti-His tag binds opsin in its tag after cell
240 permeabilization with 0.1% Triton. The Nuclei were stained with DAPI.

241

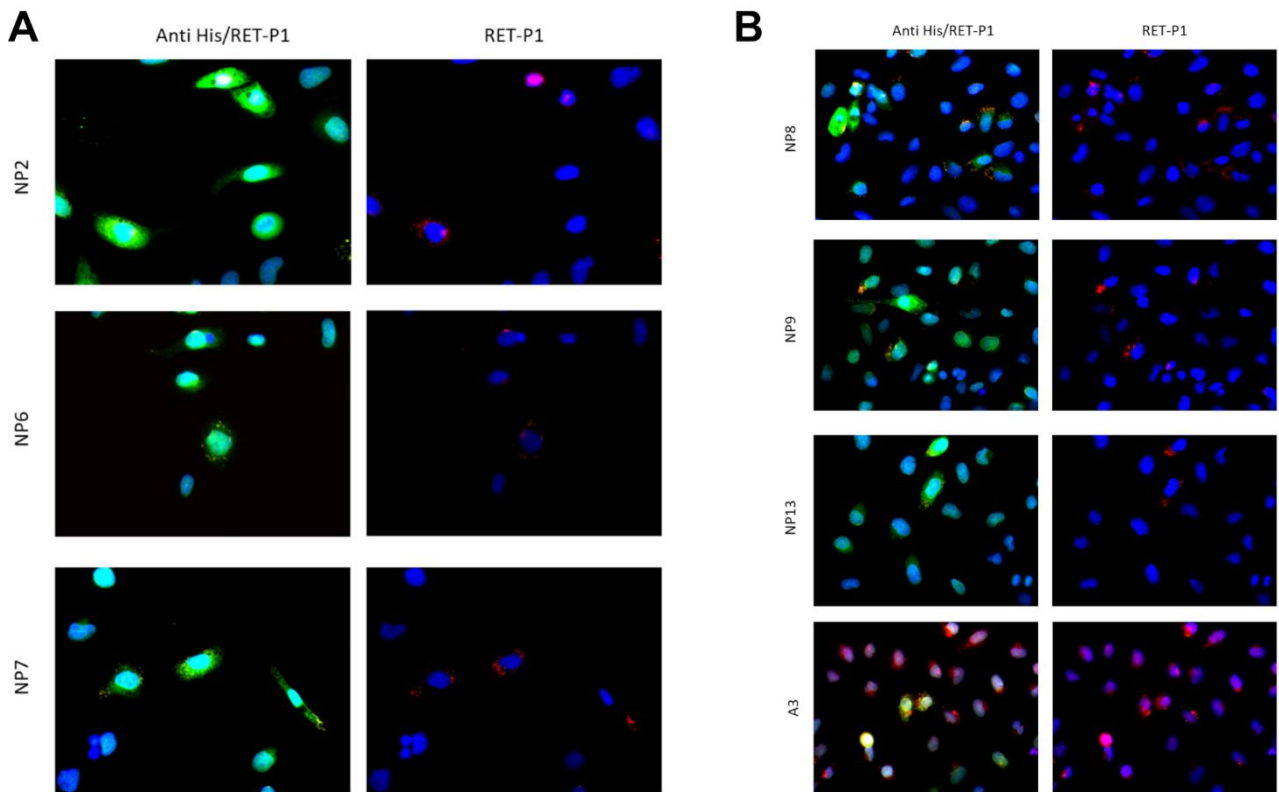
242 The screened compounds were tested at a concentration of 10 μ M, and their activity was compared
243 to the one observed for the positive (*9-cis*-retinal 5 μ M, **YC-001** 10 μ M, and beta-ionone 10 μ M)
244 and negative controls (0.1% DMSO).

245 Among the positive controls, **YC-001** appears to be similarly active to *9-cis*-retinal, while beta-
246 ionone is associated to a weaker activity (dotted red signals are visible around the membrane), even
247 though they have been both previously reported to promote opsin trafficking (Figure 8).^{21, 22, 45}

248 None of the compounds screened in this assay appeared to be as active as *9-cis*-retinal and **YC-001**.
249 However, **NP2**, **NP6**, **NP7**, **NP8**, **NP9**, **NP13** and **A3** were positive to the RET-P1 signal, although
250 opsin distribution to the cell membrane is not homogeneous but dotted and localized around the
251 nuclei as observed in beta-ionone treated cells (Figure 8). **NP5** and **A6** could not be tested because
252 insoluble at 5 mM in 100% DMSO.

253 Overall, these data corroborate the reliability of molecular modeling predictions in highlighting new
254 scaffolds, either of natural or synthetic origin, as potential chaperones of mutant opsin which might
255 be further developed as effective agents for the therapy of RP.

256



257

258 **Figure 8.** Human P23H opsin subcellular localization after U2OS treatment with 10 μ M screening
 259 compounds (NP2, NP6, NP7, NP8, NP9, NP13, A3) that resulted positive to RET-P1 staining.
 260 Anti-His/RET-P1 refers to the images merged from RET-P1 (red), and Anti-His tag (green)
 261 staining. RET-P1 refers to the images obtained from RET-P1 staining only. RET-P1 detects opsin
 262 expressed at the membrane by binding its extracellular epitope, while Anti-His tag binds opsin in its
 263 tag (C-terminus, cytosolic) after cell permeabilization with 0.1% Triton. Nuclei were stained with
 264 DAPI.

265

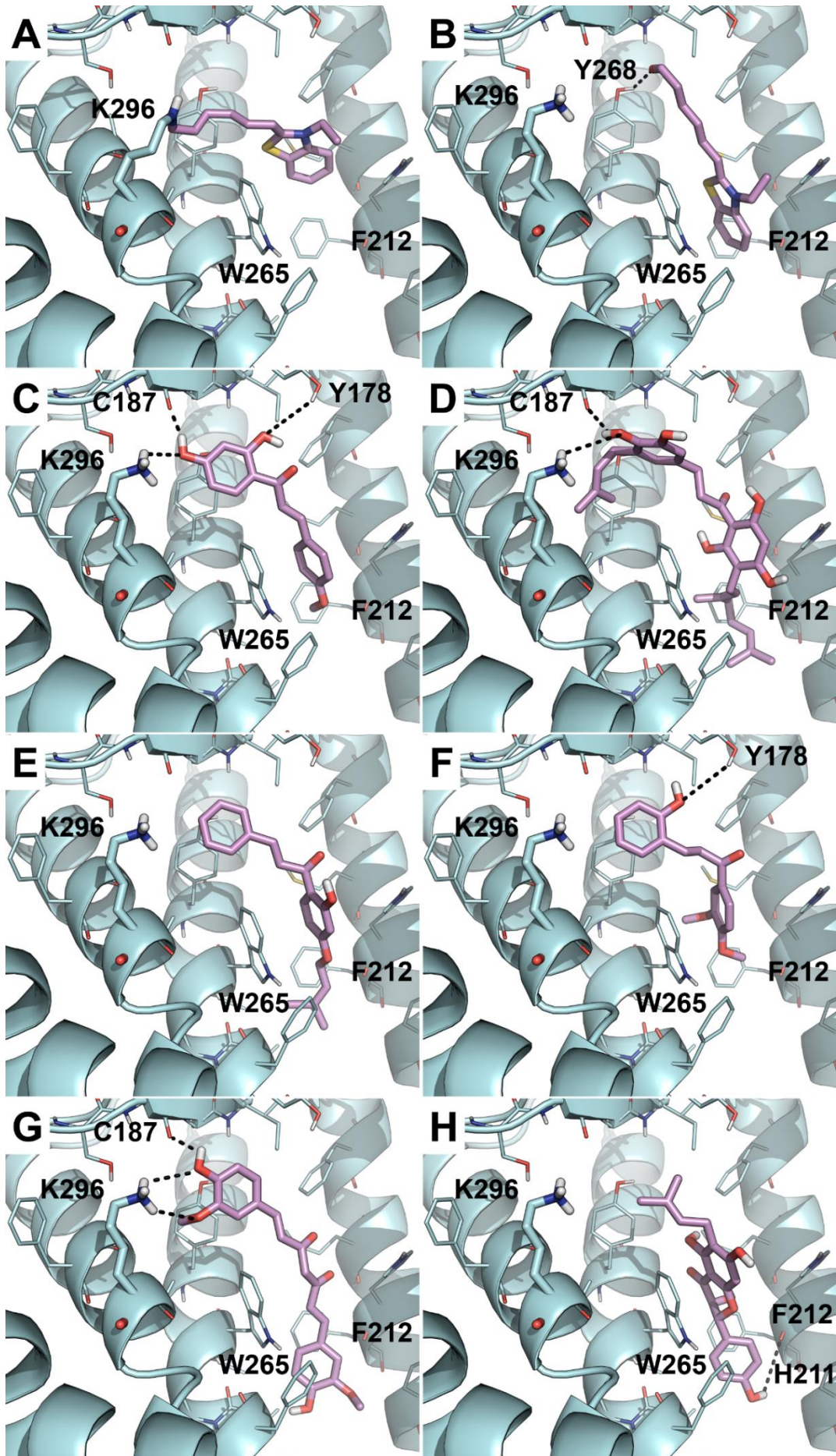
266 Predicted binding mode of molecular chaperones

267 The binding mode of the most promising molecular chaperones emerged from *in vitro* studies was
 268 further investigated by in depth molecular docking simulations. Interestingly, the aldehyde
 269 derivative A3 successfully promotes trafficking of P23H mutant opsin to the outer cell membrane
 270 and it binds similarly to 11-*cis*-retinal in docking simulations. By comparing the covalent and the

271 non-covalent docking pose of **A3** (Figure 9A and 9B), a very similar binding mode was observed,
272 although the geometry of the stacking interaction with W265 is slightly more optimized in the non-
273 covalent pose (also thanks to the sandwich with F212), most likely due to the lack of the covalent
274 bond constraints. The free aldehyde group of **A3** interacts with the side chain of Y268 in non-
275 covalent docking (Figure 9B). **NP2** belongs to the family of chalcones. Its ring B stacks over the
276 indole ring of W265 and the side chain of F212, whereas ring A is oriented toward the sidechain of
277 K296 in a geometry that corresponds to a cation-pi interaction (Figure 9C). The catechol moiety of
278 the dihydrochalcone **NP6** anchors the side chain of K296 through H-bond interactions, as well as
279 the backbone of C187. The ring A is stacked over the side chain of W265, while the lipophilic
280 geranyl chain is projected towards the inner and hydrophobic part of the TMD (Figure 9D). Nicely,
281 **NP7** adopts a binding mode that is highly overimposable to that of **NP6**, although the lack of
282 substituents in its ring B prevents any direct polar contacts to K296. Overall, the binding of **NP7**
283 within the chromophore binding site of P23H opsin seems to be driven mostly by hydrophobic
284 interactions (Figure 9E). Similarly, **NP8** fails to H-bond the side chain of K296 but the phenolic –
285 OH in ring B is H-bonded to the side chain of Y178 (Figure 9F). The aromatic core of **NP9**, i.e.,
286 curcumin, is stacked to F203 and Y206, while the substituted phenyl ring is projected toward K296
287 (Figure 9G). Although curcumin is a frequent hit in medicinal chemistry, it proved herein useful in
288 structural stabilization of the dysfunctional P23H opsin. Finally, the prenyl group of **NP13** is
289 docked near K296, whereas the aromatic core binds in proximity to F212 and it stacks over the side
290 chain of W265, this latter being one of the most conserved interactions among effective P23H
291 chaperones identified in this work (Figure 9H).

292 Overall, functional groups able to anchor K296, to stack with W265 and Y268 as well as H-bond to
293 polar residues within the chromophore binding site of P23H opsin emerged as key pharmacophores
294 for promoting opsin trafficking to the outer cell membrane.

295 To quantitatively estimate the binding affinity of non-covalent P23H opsin chaperones compared to
296 11-*cis*-retinal, MD simulations were carried out on docking complexes. The delta energy of binding
297 (ΔE_b) was then computed by the molecular mechanics/generalized Born surface area (MM-GBSA)
298 approach on MD trajectories. Results clearly suggest that most of the P23H chaperones investigated
299 herein have a ΔE_b comparable or slightly lower than 11-*cis*-retinal, with **NP6** being a stronger
300 binder than the natural chromophore (Supporting Information, Table S2).



302 **Figure 9.** Binding poses of compounds **A3** predicted by a covalent (A) and non-covalent approach
303 (B), **NP2** (C), **NP6** (D), **NP7** (E), **NP8** (F), **NP9** (G), and **NP13** (H). Small molecules are
304 represented as green sticks, P23H mutant opsin is represented as cyan cartoon and the residues
305 involved in polar or hydrophobic interactions with the small molecules are represented as cyan
306 sticks and labelled. Polar interactions are highlighted as black dashed lines.

307

308 **Conclusions**

309 In this work, a reliable computational model was developed with the aim of identifying small
310 molecules that can possibly bind the P23H opsin mutant and restore the correct protein folding and
311 localization. Computational techniques such as homology modeling and MD simulations provided a
312 fast and reliable access to structural details that are yet unavailable by structural biology and
313 prevent the identification of effective chaperones. The docking-based virtual screening of aldehydes
314 and natural products led to the identification of 20 molecules belonging to different chemical
315 classes that were selected for experimental investigations against the P23H mutant opsin.
316 Noteworthy, no approved drugs to be repurposed as P23H chaperones were identified *in silico*.
317 Single cell fluorescent microscopy and cytotoxicity assays were used to evaluate the ability of
318 selected compound to promote P23H opsin translocation to the outer cell membrane as well as to
319 preliminarily assess safety, respectively. Different natural chemotypes (**NP2**, **NP6-9**, and **NP13**)
320 and the aldehyde derivative **A3** emerged as promising molecular chaperones and structural
321 stabilizer of mutant opsin, thus validating the robustness of the computational procedure. Moreover,
322 these molecules are promising starting points for further optimization.

323

324 **Materials and methods**

325 *Homology modeling and MD simulation*

326 Since the 3D structure of the hP23H mutant rhodopsin is not solved yet, homology modelling was
327 carried out. The X-ray structure of WT bovine rhodopsin (PDB-ID: 1U19)³⁰ was selected as a
328 structural template based on its high resolution (2.20 Å), and the model was built using the Prime
329 software in the Schrödinger Release 2019-1.⁴⁶ FASTA sequences of human (Uniprot-ID: P08100)
330 and bovine (Uniprot-ID: P02699) opsin were aligned providing the 93.4% of identity of the primary
331 sequence, which provisionally allow to generate a reliable homology model.⁴⁷ The rough homology
332 model of hP23H mutant opsin in complex with the 11-*cis*-retinal covalently bound to K296 through
333 a protonated Schiff base was relaxed by MD simulation using the procedure described previously.⁴⁸
334 The ff14SB force field⁴⁹ was used to parameterized the apoprotein opsin, while the covalent bond
335 parameters of the retinal cofactor were retrieved from Ferrè et al.⁵⁰ as well as from a previous
336 work.⁴⁸ The hP23H/11-*cis*-retinal complex was then placed in a phospholipid bilayer of 138
337 molecules of 1,2-dioleoyl-sn-glycero-3-phosphocholine (DOPC)⁵¹ added by mean of the
338 CHARMM-GUI membrane builder,^{52, 53} solvated in a rectangular box of 14,629 TIP3P water
339 molecules, neutralized with the addition of 2 Na⁺ counter-ions and finally relaxed through two
340 rounds of energy minimization. The first round corresponds to energy minimization of water
341 molecules and counter-ions for 1,500 steps using the Steepest Descent algorithm (SD), and for the
342 3,500 steps using the Conjugate Gradient algorithm (CG). In the second round, energy minimization
343 of the entire system was carried out for 10,000 steps (1,500 steps SD followed by 8,500 steps CG).
344 The Langevin thermostat was then used to heat the system from 0 to 300 K over 1 ns at constant
345 volume, while the Berendsen barostat was used to control the density equilibration over 1 ns.
346 Finally, the system was preliminary equilibrated for 50 ns and MD trajectories were produced for
347 500 ns at constant pressure without restraints. MD simulations were carried out with the Amber18
348 program,⁵⁴ and the MD trajectory was analyzed by the CPPTRAJ software.⁵⁵ The hierarchical
349 agglomerative (bottom-up) approach was used to run cluster analysis on MD frames. The
350 representative MD frame of the most populated cluster was extrapolated from MD trajectory and
351 used as a rigid receptor in the docking-based virtual screening.

352

353 *Docking-based virtual Screening*

354 The docking-based virtual screening was carried out using three different libraries of compounds: i)
355 an *in house* collection of around 1,000 natural products, the Drug Bank database,³¹ and the
356 commercially available MolPort database containing 7,934,460 compounds in April 2021.³²
357 Molecules were downloaded in SMILES format and filtered through the FILTER (OpenEye)
358 version 3.1.0.3 (aldehydes were retained through the “aldehyde” rule implemented in the
359 program).⁵⁶ Compounds were converted in 3D coordinates with OMEGA (OpenEye) version
360 3.1.0.3,^{56, 57} keeping the exact stereochemistry as specified in the input file, racemic compounds or
361 molecules with unspecified chirality were discarded. The main tautomeric form of each compound
362 was retained in the virtual screening library, while the protonation state at pH 7.4 was assigned by
363 QUACKPAC (OpenEye) version 2.0.0.3.⁵⁸ Compounds were then energy minimized by SZYBKI
364 (OpenEye) version 1.10.0.3,⁵⁹ using the MMFF94S force field.⁶⁰ Non-covalent molecular docking
365 simulations of the Drug Bank database and natural products were carried out with FRED (OpenEye)
366 version 3.3.0.3^{61, 62} using the Chemgauss4 fitness function with standard settings and high docking
367 accuracy. The highest score pose of each compound was stored for visual inspection and further
368 analyses. Aldehyde compounds were docked both covalently and non-covalently using Glide XP
369 docking program from the Schrödinger Release 2019-1, using standard settings and storing the
370 highest ranking pose of each docked compound.⁶³ The pre-defined imine condensation reaction
371 between an aldehyde ligand and a lysine residue in the receptor was used in covalent docking. The
372 structure of the P23H rhodopsin mutant corresponding to the centroid of the most populated cluster
373 extracted from MD simulations was used as a rigid receptor in molecular docking simulations. ΔE_b
374 calculations were carried out with the MMPBSA.py program.⁶⁴

375

376 *Source of small molecules*

377 Aldehyde derivatives were purchased from MolPort (Riga, Latvia). Natural compounds **NP1-NP13**
378 are known structures belonging to an *in house* library of natural products, which is stored at the
379 Organic Chemistry Laboratory of the Department of Chemistry and Technology of Drugs of
380 Sapienza University of Rome. The library consists of about one thousand natural products, isolated
381 mainly from indigenous plants collected in biodiversity-rich countries, especially in tropical and
382 subtropical areas, and enlarged with their semi-synthetic and synthetic derivatives, as well as plant
383 material extracts. The chemical identity of the selected compounds was assessed by re-running
384 nuclear magnetic resonance spectroscopy (NMR) experiments and was proven to agree with the
385 literature data reported below for each compound. The purity of all compounds, checked by
386 reversed-phase high performance liquid chromatography (HPLC), was always higher than 95%.
387 Details on natural products tested in this work including source, molecular weight, and molecular
388 formula are reported in Supporting Information, Table S1). PAINS analysis of tested compounds as
389 well as SMILES strings are reported in the Supporting Information.

390 **NP1** (Emodine anthrone, 2-(3-methyl-1-butenyl)-1,8-dihydroxy-3-methoxy-6-methylanthrone
391 showed NMR spectra identical to those reported in the literature.^{65, 66} **NP2** (2',4'-dihydroxy-4-
392 methoxychalcone, (E)-1-(2,4-dihydroxyphenyl)-3-(4-methoxyphenyl)prop-2-en-1-one) showed
393 NMR spectra identical to those reported in the literature.⁶⁷ **NP3** (g-hydroxyanthrone B, (E)-1,6,8-
394 trihydroxy-4-(4-hydroxy-3-methylbut-2-en-1-yl)-3-methyl-2,5-bis(3-methylbut-2-en-1-
395 yl)anthracen-9(10H)-one) showed NMR spectra identical to those reported in the literature.⁶⁸ **NP4**
396 (Loganin, 1-((1S,4aS,6S,7R,7aS)-6-hydroxy-7-methyl-1-(((2S,3R,4S,5S,6R)-3,4,5-trihydroxy-6-
397 (hydroxymethyl)tetrahydro-2H-pyran-2-yl)oxy)-1,4a,5,6,7,7a-hexahydrocyclopenta[*c*]pyran-4-
398 yl)ethan-1-one) showed NMR spectra identical to those reported in the literature.⁶⁹ **NP5** (Sesamin,
399 5,5'-[(1S,3aR,4S,6aR)-Tetrahydro-1H,3H-furo[3,4-*c*]furan-1,4-diyl]bis(2H-1,3-benzodioxole)
400 showed NMR spectra identical to those reported in the literature.⁷⁰ **NP6** (4,2',4',6'- tetrahydroxy-
401 3'-prenyl-3-geranyldihydrochalcone, (E)-3-(3,4-dihydroxy-5-(3-methylbut-2-en-1-yl)phenyl)-1-(3-

402 (3,7-dimethylocta-2,6-dien-1-yl)-2,4,6-trihydroxyphenyl)propan-1-one) showed NMR spectra
403 identical to those reported in the literature.⁷¹ **NP7** (Cordoin, 2'-hydroxy-4'-prenylchalcone) showed
404 NMR spectra identical to those reported in the literature.⁷² **NP8** (2-hydroxy-3',4'-
405 dimethoxychalcone, (E)-1-(3,4-dimethoxyphenyl)-3-(2-hydroxyphenyl)prop-2-en-1-one) showed
406 NMR spectra identical to those reported in the literature.⁷³ **NP9** (Curcumin, (1E,6E)-1,7-bis(4-
407 hydroxy-3-methoxyphenyl)hepta-1,6-diene-3,5-dione) showed NMR spectra identical to those
408 reported in the literature.⁷⁴ **NP10** ((E)-5,7-dimethoxy-3-(4-methoxy-3-((7-methylocta-2,6-dien-1-
409 yl)oxy)phenyl)-4H-chromen-4-one) showed NMR spectra identical to those reported in the
410 literature.⁷⁵ **NP11** (Columbianetin, (S)-8-(2-hydroxypropan-2-yl)-8,9-dihydro-2H-furo[2,3-
411 h]chromen-2-one) showed NMR spectra identical to those reported in the literature.⁷⁶ **NP12** (2-
412 hydroxyderricin, 2,2'-hydroxy-4'-methoxy-3'-prenylchalcone) showed NMR spectra identical to
413 those reported in the literature.⁷⁷ **NP13** (6-prenyl-aromadendrine, 3,5,7-trihydroxy-2-(4-
414 hydroxyphenyl)-6-(3-methylbut-2-en-1-yl)chroman-4-one) showed NMR spectra identical to those
415 reported in the literature.⁷⁸

416

417 *Cell Culture*

418 ARPE-19 and U2OS cells were cultured in DMEM:F12 medium (Pan Biotech), supplemented with
419 10% foetal bovine serum (FBS) (Pan Biotech) and 1% penicillin/streptomycin (Sigma), under
420 standard cell culture conditions (in the dark, at 37.0 °C, 5% CO₂ and partial humidity).²⁸

421 Cells were harvested weekly when confluent and the media was changed every 2 days. U2OS cells
422 used in this study, stably expressing—in the presence of tetracycline—the human rhodopsin bearing
423 P23H mutation and a 6 histidines tag (His-Tag, C-terminus), have been previously described.²⁶

424 ARPE-19 (CRL-2302), human retinal pigment epithelium cells, were purchased from ATCC.

425

426 *Cell Viability Assay*

427 CellTiter-Blue Cell Viability Assay (Promega) was used to determine cell death rate after
428 compounds treatment.⁷⁹

429 Cells were harvested the day before the assay, and seeded into a 96 well plate (2x10⁴ cells/well),
430 and maintained with DMEM:F12 supplemented with 2% FBS. After 24 hours, the cells were treated
431 with 10 μ M of the tested compounds, and the following day, 20 μ l of CellTiter-Blue reagent were
432 added in each well and left to incubate at 37 °C for a maximum of 4 hours. After that, the
433 fluorescent signal was recorded using a CLARIOSTAR plate reader setting the excitation/emission
434 wavelengths to 560/590 nm. Data were normalized to 0.1% DMSO-treated cells (vehicle). The
435 fluorescence recorded from wells containing diluted reagent with media, and without the presence
436 of cells, was considered as negative control.

437

438 *Single cell fluorescent microscopy assay*

439 U2OS cells stably transfected with human P23H rhodopsin were harvested 4h before the assay and
440 plated on 13 mm coverslips precoated with poly-D-lysine (PanBiotech), then left to adhere. After
441 this period and under dim red-light conditions, the media was replaced with fresh media containing
442 1 μ g/ μ l tetracycline (Invitrogene) and of 10 μ M of the compounds (0.1% DMSO final
443 concentration).²⁸

444 Cells were incubated overnight in the dark to allow tetracycline-induced rhodopsin expression.
445 The following day, under dim-red light conditions, cells were washed twice with dPBS
446 (PanBiotech) and fixed with a solution of 4% methanol-free paraformaldehyde (Thermo Scientific)
447 for 25 minutes, followed by two PBS washes before incubating the cells with Intercept blocking
448 buffer (LI-COR) for 1h. Then, the cells were incubated with RET-P1 antibody (Invitrogene, 1:800
449 Intercept buffer) for 2h, followed by incubation with the secondary antibody anti-mouse IgG (H+L),
450 F(ab)' 2 Alexa Fluor 555 Conjugate (Cell signalling Technologies, 1:1000 Intercept Buffer), for 1h.
451 After careful repeated washing with PBS, cells were treated with a solution of 0.1% Triton for 20
452 minutes, and incubated with Anti-His Tag (Amgen, 1:500, Intercept buffer) overnight. The

453 following day, the cells were incubated with anti-mouse Ig(H+L), F(ab)² Fragment Alexa Fluor
454 488 Conjugate antibody (Cell Signalling Technologies, 1:1000 Intercept Buffer) for 1 h, washed
455 and nuclei were stained with DAPI (Sigma, 1:1000 Intercept buffer) for 10 minutes. Finally, the
456 coverslips were mounted on glass microscope slides using Moviol 488 mounting media.

457

458 **Data and Software Availability**

459 The three-dimensional structure of P23H mutant opsin extrapolated from MD simulations and used
460 in this study as a rigid receptor in virtual screening, and docking complexes of validated hit
461 compounds described in this work are available in PDB format as Supporting Information files.

462

463 **Supporting Information**

464 Additional information on compounds from the in house natural products tested in this work,
465 including source, molecular weight, and formula. PAINS analysis of tested compounds, and
466 SMILES strings.

467

468 **Acknowledgments**

469 We wish to thank the OpenEye Free Academic Licensing Programme for providing a free academic
470 license for molecular modeling and chemoinformatics software.

471

472 **Funding source**

473 The project was realized with the financial contribution of MIUR, Progetto Dipartimenti di
474 Eccellenza 2018–2022, L. 232/2016.

475

476 **References**

477 1. Kiser, P. D.; Golczak, M.; Palczewski, K., Chemistry of the retinoid (visual) cycle. *Chem*
478 *Rev* **2014**, *114*, 194-232.

- 479 2. Palczewski, K., G protein-coupled receptor rhodopsin. *Annu Rev Biochem* **2006**, *75*, 743-
480 767.
- 481 3. Ernst, O. P.; Lodowski, D. T.; Elstner, M.; Hegemann, P.; Brown, L. S.; Kandori, H.,
482 Microbial and Animal Rhodopsins: Structures, Functions, and Molecular Mechanisms. *Chem Rev*
483 **2014**, *114*, 126-163.
- 484 4. Athanasiou, D.; Aguila, M.; Bellingham, J.; Li, W. W.; McCulley, C.; Reeves, P. J.;
485 Cheetham, M. E., The molecular and cellular basis of rhodopsin retinitis pigmentosa reveals
486 potential strategies for therapy. *Prog Retin Eye Res* **2018**, *62*, 1-23.
- 487 5. Iannaccone, A.; Man, D.; Waseem, N.; Jennings, B. J.; Ganapathiraju, M.; Gallaher, K.;
488 Reese, E.; Bhattacharya, S. S.; Klein-Seetharaman, J., Retinitis pigmentosa associated with
489 rhodopsin mutations: Correlation between phenotypic variability and molecular effects. *Vision Res*
490 **2006**, *46*, 4556-4567.
- 491 6. Sung, C. H.; Davenport, C. M.; Nathans, J., Rhodopsin Mutations Responsible for
492 Autosomal-Dominant Retinitis-Pigmentosa - Clustering of Functional Classes Along the
493 Polypeptide-Chain. *J Biol Chem* **1993**, *268*, 26645-26649.
- 494 7. Chen, Y. Y.; Jastrzebska, B.; Cao, P. X.; Zhang, J. Y.; Wang, B. L.; Sun, W. Y.; Yuan, Y.
495 Y.; Feng, Z. Y.; Palczewski, K., Inherent Instability of the Retinitis Pigmentosa P23H Mutant
496 Opsin. *J Biol Chem* **2014**, *289*, 9288-9303.
- 497 8. Price, B. A.; Sandoval, I. M.; Chan, F.; Simons, D. L.; Wu, S. M.; Wensel, T. G.; Wilson, J.
498 H., Mislocalization and Degradation of Human P23H-Rhodopsin-GFP in a Knockin Mouse Model
499 of Retinitis Pigmentosa. *Invest Ophthalm Vis Sci* **2011**, *52*, 9728-9736.
- 500 9. Tam, B. M.; Moritz, O. L., Characterization of rhodopsin P23H-induced retinal degeneration
501 in a *Xenopus laevis* model of retinitis pigmentosa. *Invest Ophthalm Vis Sci* **2006**, *47*, 3234-3241.

- 502 10. Daiger, S. P., Identifying retinal disease genes: how far have we come, how far do we have
503 to go? *Novartis Found Symp* **2004**, 255, 17-27.
- 504 11. Noorwez, S. M.; Malhotra, R.; McDowell, J. H.; Smith, K. A.; Krebs, M. P.; Kaushal, S.,
505 Retinoids assist the cellular folding of the autosomal dominant retinitis pigmentosa opsin mutant
506 P23H. *J Biol Chem* **2004**, 279, 16278-16284.
- 507 12. Lin, J. H.; Li, H.; Yasumura, D.; Cohen, H. R.; Zhang, C.; Panning, B.; Shokat, K. M.;
508 Lavail, M. M.; Walter, P., IRE1 signaling affects cell fate during the unfolded protein response.
509 *Science* **2007**, 318, 944-949.
- 510 13. Kaushal, S.; Khorana, H. G., Structure and function in rhodopsin. 7. Point mutations
511 associated with autosomal dominant retinitis pigmentosa. *Biochemistry* **1994**, 33, 6121-6128.
- 512 14. Mendes, H. F.; Cheetham, M. E., Pharmacological manipulation of gain-of-function and
513 dominant-negative mechanisms in rhodopsin retinitis pigmentosa. *Hum Mol Genet* **2008**, 17, 3043-
514 3054.
- 515 15. Mendes, H. F.; van der Spuy, J.; Chapple, J. P.; Cheetham, M. E., Mechanisms of cell death
516 in rhodopsin retinitis pigmentosa: implications for therapy. *Trends Mol Med* **2005**, 11, 177-185.
- 517 16. Berson, E. L.; Rosner, B.; Sandberg, M. A.; Hayes, K. C.; Nicholson, B. W.; Weigel-
518 DiFranco, C.; Willett, W., A randomized trial of vitamin A and vitamin E supplementation for
519 retinitis pigmentosa. *Arch Ophthalmol* **1993**, 111, 761-772.
- 520 17. Ohgane, K.; Dodo, K.; Hashimoto, Y., Retinobenzaldehydes as proper-trafficking inducers
521 of folding-defective P23H rhodopsin mutant responsible for Retinitis Pigmentosa. *Bioorgan Med*
522 *Chem* **2010**, 18, 7022-7028.
- 523 18. Zhang, J. Y.; Kiser, P. D.; Badiiee, M.; Palczewska, G.; Dong, Z. Q.; Golczak, M.; Tochtrop,
524 G. P.; Palczewski, K., Molecular pharmacodynamics of emixustat in protection against retinal
525 degeneration. *Journal of Clinical Investigation* **2015**, 125, 2781-2794.

- 526 19. Kubota, R.; Boman, N. L.; David, R.; Mallikaarjun, S.; Patil, S.; Birch, D., Safety and Effect
527 on Rod Function of Acu-4429, a Novel Small-Molecule Visual Cycle Modulator. *Retina-J Ret Vit*
528 *Dis* **2012**, *32*, 183-188.
- 529 20. Behnen, P.; Felling, A.; Comitato, A.; Di Salvo, M. T.; Raimondi, F.; Gulati, S.;
530 Kahremany, S.; Palczewski, K.; Marigo, V.; Fanelli, F., A Small Chaperone Improves Folding and
531 Routing of Rhodopsin Mutants Linked to Inherited Blindness. *iScience* **2018**, *4*, 1-19.
- 532 21. Chen, Y.; Chen, Y.; Jastrzebska, B.; Golczak, M.; Gulati, S.; Tang, H.; Seibel, W.; Li, X.;
533 Jin, H.; Han, Y.; Gao, S.; Zhang, J.; Liu, X.; Heidari-Torkabadi, H.; Stewart, P. L.; Harte, W. E.;
534 Tochtrop, G. P.; Palczewski, K., A novel small molecule chaperone of rod opsin and its potential
535 therapy for retinal degeneration. *Nature communications* **2018**, *9*, 1976.
- 536 22. Matsumoto, H.; Yoshizawa, T., Existence of a beta-ionone ring-binding site in the rhodopsin
537 molecule. *Nature* **1975**, *258*, 523-526.
- 538 23. Jin, J.; Crouch, R. K.; Corson, D. W.; Katz, B. M.; MacNichol, E. F.; Cornwall, M. C.,
539 Noncovalent occupancy of the retinal-binding pocket of opsin diminishes bleaching adaptation of
540 retinal cones. *Neuron* **1993**, *11*, 513-522.
- 541 24. Noorwez, S. M.; Kuksa, V.; Imanishi, Y.; Zhu, L.; Filipek, S.; Palczewski, K.; Kaushal, S.,
542 Pharmacological chaperone-mediated in vivo folding and stabilization of the P23H-opsin mutant
543 associated with autosomal dominant retinitis pigmentosa. *J Biol Chem* **2003**, *278*, 14442-14450.
- 544 25. Vats, A.; Xi, Y.; Feng, B.; Clinger, O. D.; St Leger, A. J.; Liu, X.; Ghosh, A.; Dermond, C.
545 D.; Lathrop, K. L.; Tochtrop, G. P.; Picaud, S.; Chen, Y., Nonretinoid chaperones improve
546 rhodopsin homeostasis in a mouse model of retinitis pigmentosa. *JCI Insight* **2022**, *7(10)*: e153717.
- 547 26. Noorwez, S. M.; Ostrov, D. A.; McDowell, J. H.; Krebs, M. P.; Kaushal, S., A high-
548 throughput screening method for small-molecule pharmacologic chaperones of misfolded
549 rhodopsin. *Invest Ophthalmol Vis Sci* **2008**, *49*, 3224-3230.

- 550 27. Pasqualetto, G.; Schepelmann, M.; Varricchio, C.; Pileggi, E.; Khogali, C.; Morgan, S. R.;
551 Boostrom, I.; Rozanowska, M.; Brancale, A.; Ferla, S.; Bassetto, M., Computational Studies
552 towards the Identification of Novel Rhodopsin-Binding Compounds as Chemical Chaperones for
553 Misfolded Opsins. *Molecules* **2020**, *25* (21): 4904.
- 554 28. Pasqualetto, G.; Pileggi, E.; Schepelmann, M.; Varricchio, C.; Rozanowska, M.; Brancale,
555 A.; Bassetto, M., Ligand-based rational design, synthesis and evaluation of novel potential chemical
556 chaperones for opsin. *Eur J Med Chem* **2021**, *226*, 113841.
- 557 29. Berman, H. M.; Westbrook, J.; Feng, Z.; Gilliland, G.; Bhat, T. N.; Weissig, H.; Shindyalov,
558 I. N.; Bourne, P. E., The Protein Data Bank. *Nucleic Acids Res* **2000**, *28*, 235-242.
- 559 30. Okada, T.; Sugihara, M.; Bondar, A. N.; Elstner, M.; Entel, P.; Buss, V., The retinal
560 conformation and its environment in rhodopsin in light of a new 2.2 Å crystal structure. *Journal of*
561 *molecular biology* **2004**, *342*, 571-583.
- 562 31. Wishart, D. S.; Knox, C.; Guo, A. C.; Shrivastava, S.; Hassanali, M.; Stothard, P.; Chang,
563 Z.; Woolsey, J., DrugBank: a comprehensive resource for in silico drug discovery and exploration.
564 *Nucleic Acids Res* **2006**, *34*, D668-D672.
- 565 32. Easy compound ordering service - MolPort. <https://www.molport.com/shop/index>.
- 566 33. Newman, D. J.; Cragg, G. M., Natural Products as Sources of New Drugs over the Nearly
567 Four Decades from 01/1981 to 09/2019. *Journal of natural products* **2020**, *83*, 770-803.
- 568 34. Ghirga, F.; Quaglio, D.; Mori, M.; Cammarone, S.; Iazzetti, A.; Goggiamani, A.; Ingallina,
569 C.; Botta, B.; Calcaterra, A., A unique high-diversity natural product collection as a reservoir of
570 new therapeutic leads. *Organic Chemistry Frontiers* **2021**, *8*, 996-1025.
- 571 35. Platella, C.; Ghirga, F.; Zizza, P.; Pompili, L.; Marzano, S.; Pagano, B.; Quaglio, D.;
572 Vergine, V.; Cammarone, S.; Botta, B.; Biroccio, A.; Mori, M.; Montesarchio, D., Identification of

573 Effective Anticancer G-Quadruplex-Targeting Chemotypes through the Exploration of a High
574 Diversity Library of Natural Compounds. *Pharmaceutics* **2021**, *13* (10):1611.

575 36. Zheng, Y.; Yang, X. W.; Schols, D.; Mori, M.; Botta, B.; Chevigne, A.; Mulinge, M.;
576 Steinmetz, A.; Schmit, J. C.; Seguin-Devaux, C., Active Components from *Cassia abbreviata*
577 Prevent HIV-1 Entry by Distinct Mechanisms of Action. *International journal of molecular*
578 *sciences* **2021**, *22*, 5052.

579 37. Quaglio, D.; Mangoni, M. L.; Stefanelli, R.; Corradi, S.; Casciaro, B.; Vergine, V.;
580 Lucantoni, F.; Cavinato, L.; Cammarone, S.; Loffredo, M. R.; Cappiello, F.; Calcaterra, A.; Erazo,
581 S.; Ghirga, F.; Mori, M.; Imperi, F.; Ascenzioni, F.; Botta, B., ent-Beyerane Diterpenes as a Key
582 Platform for the Development of ArnT-Mediated Colistin Resistance Inhibitors. *J Org Chem* **2020**,
583 *85*, 10891-10901.

584 38. Mascarello, A.; Orbem Menegatti, A. C.; Calcaterra, A.; Martins, P. G. A.; Chiaradia-
585 Delatorre, L. D.; D'Acquarica, I.; Ferrari, F.; Pau, V.; Sanna, A.; De Logu, A.; Botta, M.; Botta, B.;
586 Terenzi, H.; Mori, M., Naturally occurring Diels-Alder-type adducts from *Morus nigra* as potent
587 inhibitors of *Mycobacterium tuberculosis* protein tyrosine phosphatase B. *European journal of*
588 *medicinal chemistry* **2018**, *144*, 277-288.

589 39. Mori, M.; Kovalenko, L.; Malancona, S.; Saladini, F.; De Forni, D.; Pires, M.; Humbert, N.;
590 Real, E.; Botzanowski, T.; Cianferani, S.; Giannini, A.; Dasso Lang, M. C.; Cugia, G.; Poddesu, B.;
591 Lori, F.; Zazzi, M.; Harper, S.; Summa, V.; Mely, Y.; Botta, M., Structure-Based Identification of
592 HIV-1 Nucleocapsid Protein Inhibitors Active against Wild-Type and Drug-Resistant HIV-1
593 Strains. *ACS chemical biology* **2018**, *13*, 253-266.

594 40. Mori, M.; Tottone, L.; Quaglio, D.; Zhdanovskaya, N.; Ingallina, C.; Fusto, M.; Ghirga, F.;
595 Peruzzi, G.; Crestoni, M. E.; Simeoni, F.; Giulimondi, F.; Talora, C.; Botta, B.; Screpanti, I.;
596 Palermo, R., Identification of a novel chalcone derivative that inhibits Notch signaling in T-cell
597 acute lymphoblastic leukemia. *Scientific reports* **2017**, *7*, 2213.

- 598 41. Pushpakom, S.; Iorio, F.; Eyers, P. A.; Escott, K. J.; Hopper, S.; Wells, A.; Doig, A.;
599 Guilliams, T.; Latimer, J.; McNamee, C.; Norris, A.; Sanseau, P.; Cavalla, D.; Pirmohamed, M.,
600 Drug repurposing: progress, challenges and recommendations. *Nat Rev Drug Discov* **2019**, *18*, 41-
601 58.
- 602 42. Pillaiyar, T.; Meenakshisundaram, S.; Manickam, M.; Sankaranarayanan, M., A medicinal
603 chemistry perspective of drug repositioning: Recent advances and challenges in drug discovery. *Eur*
604 *J Med Chem* **2020**, *195*, 112275.
- 605 43. Cusinato, J.; Cau, Y.; Calvani, A. M.; Mori, M., Repurposing drugs for the management of
606 COVID-19. *Expert Opin Ther Pat* **2021**, *31*, 295-307.
- 607 44. Palczewski, K., Retinoids for treatment of retinal diseases. *Trends in pharmacological*
608 *sciences* **2010**, *31*, 284-295.
- 609 45. Makino, C. L.; Riley, C. K.; Looney, J.; Crouch, R. K.; Okada, T., Binding of more than one
610 retinoid to visual opsins. *Biophysical journal* **2010**, *99*, 2366-2373.
- 611 46. Jacobson, M. P.; Pincus, D. L.; Rapp, C. S.; Day, T. J.; Honig, B.; Shaw, D. E.; Friesner, R.
612 A., A hierarchical approach to all-atom protein loop prediction. *Proteins* **2004**, *55*, 351-367.
- 613 47. Rost, B., Twilight zone of protein sequence alignments. *Protein Eng* **1999**, *12*, 85-94.
- 614 48. Picarazzi, F.; Manetti, F.; Marigo, V.; Mori, M., Conformational insights into the C-terminal
615 mutations of human rhodopsin in retinitis pigmentosa. *Journal of molecular graphics & modelling*
616 **2022**, *110*, 108076.
- 617 49. Maier, J. A.; Martinez, C.; Kasavajhala, K.; Wickstrom, L.; Hauser, K. E.; Simmerling, C.,
618 ff14SB: Improving the Accuracy of Protein Side Chain and Backbone Parameters from ff99SB. *J*
619 *Chem Theory Comput* **2015**, *11*, 3696-3713.

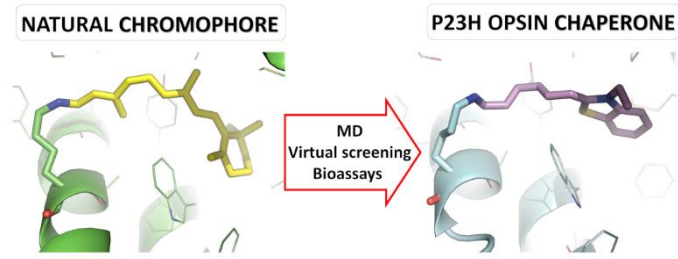
- 620 50. Ferré, N.; Cembran, A.; Garavelli, M.; Olivucci, M., Complete-active-space self-consistent-
621 field/Amber parameterization of the Lys296–retinal–Glu113 rhodopsin chromophore-counterion
622 system. *Theoretical Chemistry Accounts* **2004**, *112*, 335-341.
- 623 51. Kong, Y.; Karplus, M., The signaling pathway of rhodopsin. *Structure* **2007**, *15*, 611-23.
- 624 52. Jo, S.; Kim, T.; Iyer, V. G.; Im, W., CHARMM-GUI: a web-based graphical user interface
625 for CHARMM. *Journal of computational chemistry* **2008**, *29*, 1859-1865.
- 626 53. Lee, J.; Hitzenberger, M.; Rieger, M.; Kern, N. R.; Zacharias, M.; Im, W., CHARMM-GUI
627 supports the Amber force fields. *The Journal of Chemical Physics* **2020**, *153*, 035103.
- 628 54. Case, D. A.; Cheatham, T. E., 3rd; Darden, T.; Gohlke, H.; Luo, R.; Merz, K. M., Jr.;
629 Onufriev, A.; Simmerling, C.; Wang, B.; Woods, R. J., The Amber biomolecular simulation
630 programs. *J Comput Chem* **2005**, *26*, 1668-1688.
- 631 55. Roe, D. R.; Cheatham, T. E., 3rd, PTRAJ and CPPTRAJ: Software for Processing and
632 Analysis of Molecular Dynamics Trajectory Data. *J Chem Theory Comput* **2013**, *9*, 3084-3095.
- 633 56. Hawkins, P. C.; Skillman, A. G.; Warren, G. L.; Ellingson, B. A.; Stahl, M. T., Conformer
634 generation with OMEGA: algorithm and validation using high quality structures from the Protein
635 Databank and Cambridge Structural Database. *J Chem Inf Model* **2010**, *50*, 572-584.
- 636 57. *OMEGA 3.1.0.3: OpenEye Scientific Software, Santa Fe, NM. <http://www.eyesopen.com>.*
- 637 58. *QUACPAC 2.0.0.3: OpenEye Scientific Software, Santa Fe, NM. <http://www.eyesopen.com>.*
- 638 59. *SZYBKI 1.10.0.3: OpenEye Scientific Software, Santa Fe, NM. <http://www.eyesopen.com>.*
- 639 60. Halgren, T. A., MMFF VI. MMFF94s option for energy minimization studies. *Journal of*
640 *computational chemistry* **1999**, *20*, 720-729.
- 641 61. McGann, M., FRED pose prediction and virtual screening accuracy. *J Chem Inf Model*
642 **2011**, *51*, 578-596.

- 643 62. *OEDOCKING 3.3.0.3: OpenEye Scientific Software, Inc., Santa Fe, NM.*
644 <http://www.eyesopen.com>.
- 645 63. Friesner, R. A.; Murphy, R. B.; Repasky, M. P.; Frye, L. L.; Greenwood, J. R.; Halgren, T.
646 A.; Sanschagrin, P. C.; Mainz, D. T., Extra precision glide: docking and scoring incorporating a
647 model of hydrophobic enclosure for protein-ligand complexes. *Journal of medicinal chemistry*
648 **2006**, *49*, 6177-6196.
- 649 64. Miller, B. R.; McGee, T. D.; Swails, J. M.; Homeyer, N.; Gohlke, H.; Roitberg, A. E.,
650 MMPBSA.py: An Efficient Program for End-State Free Energy Calculations. *J Chem Theory*
651 *Comput* **2012**, *8*, 3314-3321.
- 652 65. Iinuma, M.; Tosa, H.; Ito, T.; Tanaka, T.; Aqil, M., 2 Prenylated Anthrones in Harungana-
653 Madagascariensis. *Phytochemistry* **1995**, *40*, 267-270.
- 654 66. Delle Monache, F.; Ferrari, F.; Marini-Bettolo, G. B., Vismiones from *Vismia baccifera* var.
655 dealdata (H.B.K.): chemistry and X-ray structure determination. *Gazz Chim Ital* **1979**, *109*, 301-
656 309.
- 657 67. Severi, F.; Benvenuti, S.; Costantino, L.; Vampa, G.; Melegari, M.; Antolini, L., Synthesis
658 and activity of a new series of chalcones as aldose reductase inhibitors. *Eur J Med Chem* **1998**, *33*,
659 859-866.
- 660 68. Moura Pinheiro, R.; Marquina Mac-Quhae, M.; Marini-Bettolo, G. B.; Delle Monache, F.,
661 Prenylated anthranoids from *Vismia species*. *Phytochemistry* **1984**, *23*, 1737-1740.
- 662 69. Garcia, J.; Chulia, A. J., Loganin and new iridoid glucosides in *Gentiana pedicellata*. *Planta*
663 *Med* **1986**, 327-329.
- 664 70. Lin, C. L.; Kao, C. L.; Li, W. J.; Li, H. T.; Chen, C. Y., SECONDARY METABOLITES
665 FROM THE STEMS OF *Cinnamomum kanehirai*. *Chem Nat Compd* **2018**, *54*, 762-763.

- 666 71. Trani, M.; Delle Monache, F.; Delle Monache, G.; Yunes, R. A.; Falkenberg, D. B.,
667 Dihydrochalcones and coumarins of *Esembeckia grandiflora* subsp. *grandiflora*. *Gazz Chim Ital*
668 **1997**, *127*, 415-418.
- 669 72. De Lima, O. G.; Marini-Bettolo, G. B.; De Mello, J. F.; Delle Monache, F.; Coêlho, J. S. D.
670 B.; Lyra, F. D. D. A.; De Albuquerque, M. M. F., Cordoia: primo esempio di una nuova classe di
671 calconi naturali O-prenilati. *Atti della Accademia Nazionale dei Lincei. Classe di Scienze Fisiche,*
672 *Matematiche e Naturali. Rendiconti* **1972**, *53*, 433-435.
- 673 73. Maccarone, E.; Cuffari, G.; Passerini, A.; Raymo, F., Diphenyl Ethers from 2-
674 Hydroxychalcone Precursors of Flavylum Salts. *J Chem Res-S* **1991**, 240-241.
- 675 74. Payton, F.; Sandusky, P.; Alworth, W. L., NMR study of the solution structure of curcumin.
676 *J Nat Prod* **2007**, *70*, 143-146.
- 677 75. Berardozi, S.; Bernardi, F.; Infante, P.; Ingallina, C.; Toscano, S.; De Paolis, E.; Alfonsi,
678 R.; Caimano, M.; Botta, B.; Mori, M.; Di Marcotullio, L.; Ghirga, F., Synergistic inhibition of the
679 Hedgehog pathway by newly designed Smo and Gli antagonists bearing the isoflavone scaffold. *Eur*
680 *J Med Chem* **2018**, *156*, 554-562.
- 681 76. Magolan, J.; Coster, M. J., Total synthesis of (+)-angelmarin. *J Org Chem* **2009**, *74*, 5083-
682 5086.
- 683 77. Lupi, A.; Delle Monache, G.; Delle Monache, F.; Marini-Bettolo, G. B.; Goncalves de Lima,
684 O.; De Mello, J. F., Synthetic analogs of natural prenylated and chromene chalcones. *Farmaco Sci*
685 **1977**, *32*, 261-269.
- 686 78. Fukai, T.; Nomura, T., ¹H NMR Spectra of Prenylated Flavonoids and Pyranoflavonoids.
687 *Heterocycles* **1993**, *36*, 329-343.
- 688 79. Stoddart, M. J., Cell viability assays: introduction. *Methods in molecular biology* **2011**, *740*,
689 1-6.

690

For Table of Contents Use Only



691